Chapter 3
Basic Theory of Piezotronics

Abstract Using the basic transport equations, this chapter gives the theory of charge transport in piezotronic devices. Besides presenting the formal theoretical frame work, analytical solutions are presented for cases like the metal–semiconductor contact and p–n junction under simplified conditions. Numerical calculations are given for predicting the current–voltage characteristics of a general piezotronic transistor: metal–ZnO nanowire–metal device. This study is important for understanding the working principle and characteristics of piezotronic devices, but also for providing guidance for device design.

Due to the coupling of piezoelectric and semiconducting properties, nano/microwires of piezoelectric semiconductor have been used as basic building blocks for fabricating various innovative devices, such as nanogenerators [1–3], piezoelectric field effect transistors [4], piezoelectric diodes [5], piezoelectric chemical sensors [6], and piezo-phototronic devices [7, 8]. Take a ZnO nanowire as an example. When a tensile strain is applied along the nanowire that grows in the *c*-axis direction, piezoelectric charges are created at its two ends, forming a piezoelectric potential inside the nanowire. This potential tunes the contact of the nanowire with the electrodes by changing the height of the local Schottky barrier, thus, the transport behavior of the charge carriers in the nanowire is controlled/tuned by the externally applied strain. This is the piezotronic effect. Electronics fabricated by using the inner-crystal piezopotential as a "gate" voltage to tune/control the charge transport behavior across a metal–semiconductor interface or a p–n junction is named *piezotronics*, which is different from the basic design of CMOS field effect transistor, and it has applications in force/pressure triggered/controlled electronic devices, sensors, MEMS, human–computer interfacing, nanorobotics and touch-pad technologies.

In this chapter, we present a fundamental theoretical framework of piezotronics for understanding and quantitatively calculating the carrier transport behavior in the devices [9]. We first give some analytical solutions for ZnO piezoelectric p–n junction and metal–semiconductor (M–S) contact under simplified conditions, which are useful for understanding the piezotronic behavior in general. Furthermore, using the FEM, the characteristics of a piezotronic transistor, ZnO nanowire metal–semiconductor–metal (M–S–M) structure, are simulated. The theoretical re-

Z.L. Wang, *Piezotronics and Piezo-Phototronics*, Microtechnology and MEMS,
DOI 10.1007/978-3-642-34237-0_3, © Springer-Verlag Berlin Heidelberg 2012

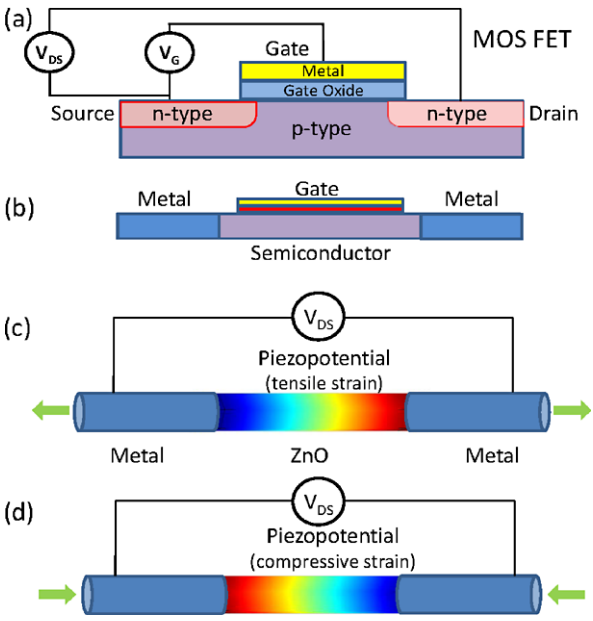

Fig. 3.1 Schematic of (**a**) an n-channel MOS FET and (**b**) a semiconductor nanowire FET; schematic of a piezotronic transistor with tensile strain (**c**) and compressive strain (**d**), where the gate voltage that controls the channel width is replaced by a piezopotential that controls the transport across the metal–semiconductor interface [9]

sults establish the basic physics for understanding the observed experimental results from piezotronic devices and guiding future device design.

3.1 Piezotronic Transistor vs. Traditional Field Effect Transistor

In order to illustrate the basic concept of piezotronics, we first start from a traditional metal oxide semiconductor field-effect transistor (MOS FET). For an n-channel MOS FET (Fig. 3.1(a)), the two n-type doped regions are the drain and source; a thin insulator oxide layer is deposited on the p-type region to serve as the gate oxide, on which a metal contact is made as the gate. The current flowing from the drain to source under an applied external voltage V_{DS} is controlled by the gate voltage V_G, which controls the channel width for transporting the charge carriers. In analogy, for a single channel FET fabricated using a semiconductor NW (Fig. 3.1(b)), the drain and source are the two metal electrodes at the two ends, and a gate voltage is applied at the top of the NW or through the base substrate.

A piezotronic transistor is a metal–NW–metal structure, such as Au–ZnO–Au or Ag–ZnO–Ag as shown in Fig. 3.1(c) and (d) [9]. The fundamental principle of the piezotronic transistor is to control the carrier transport at the M–S interface through a tuning at the local contact by creating a piezopotential at the interface region in the semiconductor by applying a strain. This structure is different from the CMOS design as stated in follows. First, the externally applied gate voltage is replaced by an inner-crystal potential generated by piezoelectric effect, thus, the "gate" electrode is eliminated. This means that the piezotronic transistor only has two leads: drain and

source. Secondly, the control over channel width is replaced by a control at the interface. Since the current transported across a M–S interface is the exponential of the local barrier height at the reversely biased case, the ON and OFF ratio can be rather high due to the non-linear effect. Finally, a voltage controlled device is replaced by an external strain/stress controlled device, which is likely to have complementary applications to CMOS devices.

When a ZnO NW device is under strain, there are two typical effects that may affect the carrier transport process. One is the piezoresistance effect because of the change in band gap, charge carrier density and possibly density of states in the conduction band of the semiconductor crystal under strain. This effect is a symmetric effect on the two end contact and has no polarity, which will not produce the function of a transistor. Piezoresistance is a common feature of any semiconductors such as Si and GaAs and is not limited to the wurtzite family. The other is the piezoelectric effect because of the polarization of ions in a crystal that has non-central symmetry, which has an asymmetric or non-symmetric effect on the local contacts at the source and drain owing to the polarity of the piezopotential. In general, the negative piezopotential side raises the barrier height at the local contact of metal n-type semiconductor, possibly changing a Ohmic contact to a Schottky contact, a Schottky contact to an "insulator" contact; while the positive piezopotential side lowers the local barrier height, changing a Schottky contact to an Ohmic contact. But the degree of changes in the barrier heights depends on the doping type and doping density in the NW. The piezoelectric charges are located at the ends of the wire, thus they directly affect the local contacts. The piezotronic effect is likely limited to the wurtzite family such as ZnO, GaN, CdS and InN. It is important to point out that the polarity of the piezopotential can be switched by changing tensile strain to compressive strain. Thus, the device can be changed from a control at source to a control at drain simply by reversing the sign of strain applied to the device.

3.2 Effect of Piezopotential on Metal–Semiconductor Contact

When a metal and a n-type semiconductor forms a contact, a Schottky barrier (SB) ($e\phi_{SB}$) is created at the interface if the work function of the metal is appreciably larger than the electron affinity of the semiconductor (Fig. 3.2(a)). Current can only pass through this barrier if the applied external voltage is larger than a threshold value (ϕ_i) and its polarity is at the metal side positive (for n-type semiconductor). If a photon excitation is applied at the interface, the newly generated electrons in conduction band tend to move away from the contact, while the holes tend to move close to the interface toward the metal side. The accumulated holes at the interface modify the local potential profile, so that the effective height of the Schottky barrier is lowered (Fig. 3.2(b)), which increases the conductance.

Once a strain is created in a semiconductor that also has the piezoelectric property, a negative piezopotential at the semiconductor side effectively increases the local SB height to $e\phi'$ (Fig. 3.2(c)) [10], while a positive piezopotential reduces

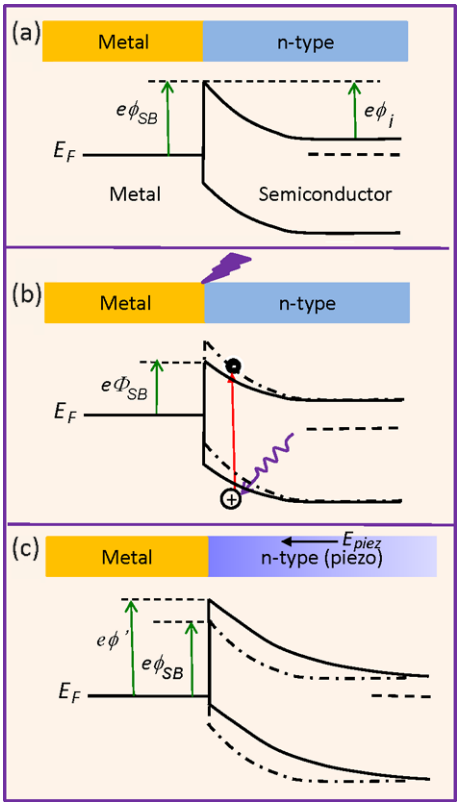

Fig. 3.2 Energy band diagram for illustrating the effects of laser excitation and piezoelectricity on a Schottky contacted metal–semiconductor interface. (**a**) Band diagram at a Schottky contacted metal–semiconductor interface. (**b**) Band diagram at a Schottky contact after exciting by a laser that has a photon energy higher than the bandgap, which is equivalent to a reduction in the Schottky barrier height. (**c**) Band diagram at the Schottky contact after applying a strain in the semiconductor. The piezopotential created in the semiconductor has a polarity with the end in contact with the metal being low [10]

the barrier height. The role played by the piezopotential is to effectively change the local contact characteristics through an internal field depending on the crystallographic orientation of the material and the sign of the strain, thus, the charge carrier transport process is tuned/gated at the metal–semiconductor (M–S) contact. Considering the change in piezopotential polarity by switching the strain from tensile to compressive, the local contact characteristics can be tuned and controlled by the magnitude of the strain and the sign of strain [11]. Therefore, the charge transport across the interface can be largely dictated by the created piezopotential, which is the gate effect. This is the core of piezotronics.

On the other hand, if we excited a MS contact by photons that have an energy larger than the bandgap of the semiconductor, electron-hole pairs are generated at the vicinity of the contact. The presence of free carriers at the interface can effectively reduce the Schottky-barrier height. Therefore, piezopotential can increase the local barrier height, while laser excitation can effectively reduce the local barrier height. The two effects can be applied in a complementary way for controlling the charge transport at the interface. This is a coupling between piezoelectricity and photon excitation.

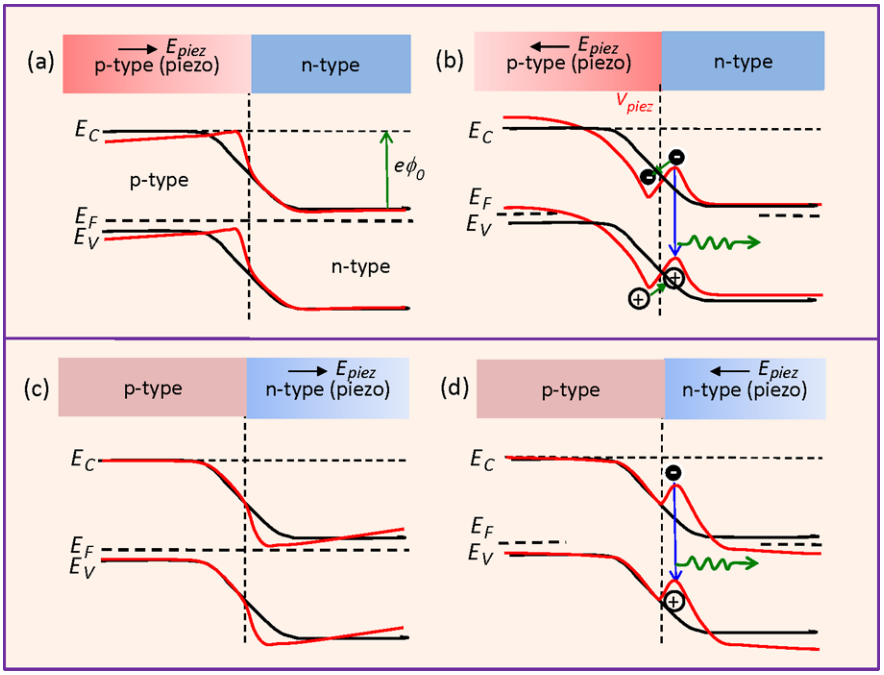

Fig. 3.3 Energy band diagram for illustrating the effect of piezoelectricity on a p–n junction that is made of two materials of similar bandgaps. The band diagrams for the p–n junction with and without the presence of piezoelectric effect for the four possible cases are shown using dark and red curves, respectively. The bandgap for the n-type and p-type are assumed to be about equal. The effect of reversal in polarity is presented [10]

3.3 Effect of Piezopotential on p–n Junction

When a p-type and a n-type semiconductors form a junction, the holes in the p-type side and the electrons in the n-type side tend to redistribute to balance the local potential, the interdiffusion and recombination of the electrons and holes in the junction region forms a charge depletion zone. The presence of such a carrier free zone can significantly enhance the piezoelectric effect, because the piezo-charges will be mostly preserved without being screened by local residual free carriers. As shown in Fig. 3.3(a), for a case that the p-type side is piezoelectric and a strain is applied, local net negative piezo-charges are preserved at the junction provided the doping is relatively low so that the local free carriers are not enough to fully screen the piezo-charges. The piezopotential tends to raise the local band slightly and introduce a slow slope to the band structure. Alternatively, if the applied strain is switched in sign (Fig. 3.3(b)), the positive piezo-charges at the interface creates a dip in the local band. A modification in the local band may be effective for trapping the holes so that the electron-hole recombination rate can be largely enhanced, which is very beneficial for improving the efficiency of an LED [12]. Furthermore, the inclined band tends to change the mobility of the carriers moving toward the junction.

By the same token, if the n-type side is piezoelectric, a similar band structure change can be induced from the piezoelectric effect, as shown in Figs. 3.3(c), (d). The band structure modification at the interface/junction by piezoelectric charges introduces some fundamental changes to the local band structure, which is effective for controlling the device performance.

For a p–n junction made of two materials with distinctly different bandgaps, local piezo-charges can also significantly affect the band profile, as shown in Fig. 3.4 [13], so that the transport of the charge carriers across the interface will be significantly modified. Take the case shown in Fig. 3.4(e) as an example: the barrier height at the interface as created by band misalignment can be reduced so that the electrons can be effectively transported across the interface. For the case of Fig. 3.4(f), the height and width of the barrier at the interface are increased by piezo-charges. As for the case presented in Fig. 3.4(b), the local trapping of holes can be significantly increased, which may be beneficial for LED. But for the case in Fig. 3.4(a), it may have negative effect on LED efficiency. Therefore, the presence of piezo-charges at the junction can be useful for some optoelectronic processes.

3.4 Theoretical Frame of the Piezotronic Effect

Since a piezotronic transistor involves a semiconductor that is piezoelectric, the fundamental governing equations for both semiconductor and piezoelectric theories are required. The basic equations for piezotronics are electrostatic equations, current–density equations, and continuity equations, which describe the static and dynamic transport behavior of the charge carriers in semiconductors [14–16], as well as the piezoelectric equations, which describe the piezoelectric behavior of the material under dynamic straining [18].

The Poisson equation is the basic equation for describing the electrostatic behavior of charges:

$$\nabla^2 \psi_i = -\frac{\rho(\mathbf{r})}{\varepsilon_s} \tag{3.1}$$

where ψ_i is the electric potential distribution and $\rho(\mathbf{r})$ is the charge density distribution, ε_s is the permittivity of the material.

The current–density equations that correlate the local fields, charge densities and local currents are

$$\begin{cases} \mathbf{J}_n = q\mu_n n\mathbf{E} + qD_n \nabla n, \\ \mathbf{J}_p = q\mu_p p\mathbf{E} - qD_p \nabla p, \\ \mathbf{J}_{\text{cond}} = \mathbf{J}_n + \mathbf{J}_p \end{cases} \tag{3.2}$$

where $\mathbf{J}_n$ and $\mathbf{J}_p$ are the electron and hole current densities, q is the absolute value of unit electronic charge, μ_n and μ_p are electron and hole mobilities, n and p are concentrations of free electrons and free holes, D_n and D_p are diffusion coefficients for electrons and holes, respectively, $\mathbf{E}$ is the electric field, and $\mathbf{J}_{\text{cond}}$ is the total current density.

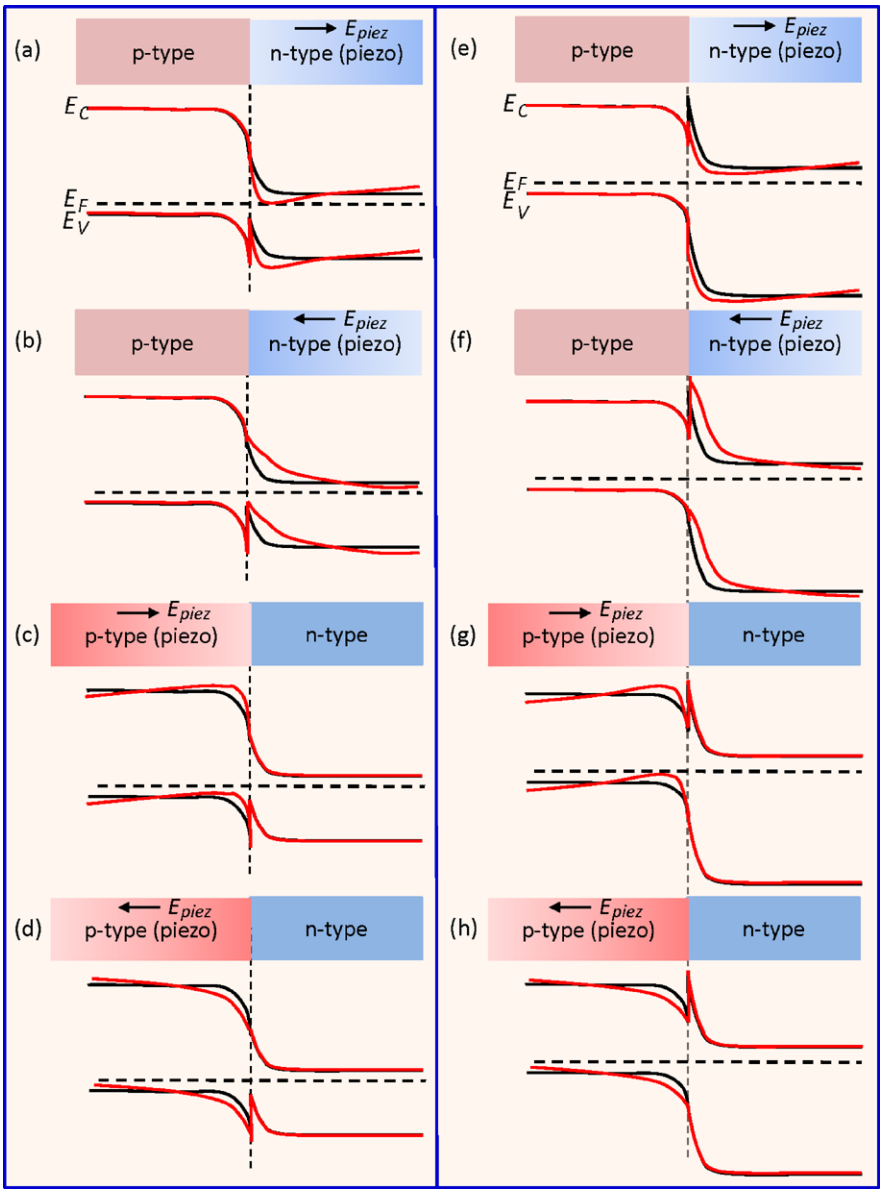

Fig. 3.4 Energy band diagram for illustrating the effect of piezoelectricity on a heterostructured p–n junction. The band diagrams for the p–n junction with and without the presence of piezoelectric effect for the eight possible cases are shown using *dark* and *red curves*, respectively. The effect of reversal in polarity is also presented [13]

The charge transport under the driving of a field is described by the continuity equations.

$$\begin{cases} \dfrac{\partial n}{\partial t} = G_n - U_n + \dfrac{1}{q}\nabla \cdot \mathbf{J}_n, \\ \dfrac{\partial p}{\partial t} = G_p - U_p - \dfrac{1}{q}\nabla \cdot \mathbf{J}_p \end{cases} \tag{3.3}$$

where G_n and G_p are the electron and hole generation rates, U_n and U_p are the recombination rates, respectively.

The piezoelectric behavior of the material is described by a polarization vector $\mathbf{P}$. For a small uniform mechanical strain S_{ik}, the polarization $\mathbf{P}$ vector is given in terms of strain $\mathbf{S}$ as

$$(\mathbf{P})_i = (\mathbf{e})_{ijk}(\mathbf{S})_{jk} \tag{3.4}$$

where the third order tensor $(\mathbf{e})_{ijk}$ is the piezoelectric tensor. According to the conventional theory of piezoelectric and elasticity, the constituting equations can be written as

$$\begin{cases} \boldsymbol{\sigma} = \mathbf{c}_E\mathbf{S} - \mathbf{e}^{\mathbf{T}}\mathbf{E}, \\ \mathbf{D} = \mathbf{e}\mathbf{S} + \mathbf{k}\mathbf{E} \end{cases} \tag{3.5}$$

where $\boldsymbol{\sigma}$ is the stress tensor, $\mathbf{E}$ is the electric field, $\mathbf{D}$ is the electric displacement, $\mathbf{c}_E$ is the elasticity tensor, and $\mathbf{k}$ is the dielectric tensor.

3.5 Analytical Solution for One-Dimensional Simplified Cases

In practical device modeling, the above basic equations can be solved under specific boundary conditions. For simplicity of illustrating the basic physics, we consider an one-dimension piezotronic device with ideal Ohmic contacts at the source and drain. This means that the Dirichlet boundary conditions of the carrier concentration and electrical potential will be applied at the device boundaries. The strain is applied normal to the M–S interface without introducing shear strain.

3.5.1 Piezoelectric p–n Junctions

The p–n junctions are most fundamental building blocks in modern electronic devices. Shockley theory provides the basic theory of current–voltage (I–V) characteristics of the p–n junctions. For better understanding about piezoelectric p–n junction, we describe the physics of the semiconductor using Shockley theory. For simplicity, we assume that the p-type region is non-piezoelectric and the n-type region is piezoelectric. Considering that ZnO grows along the direction of c-axis, the positive charges are created at the n-type side of the p–n junction by applying a compressive stress along the c-axis. For convenience in using piezoelectric theory, the piezoelectric charges are considered as surface charge at the bulk piezoelectric

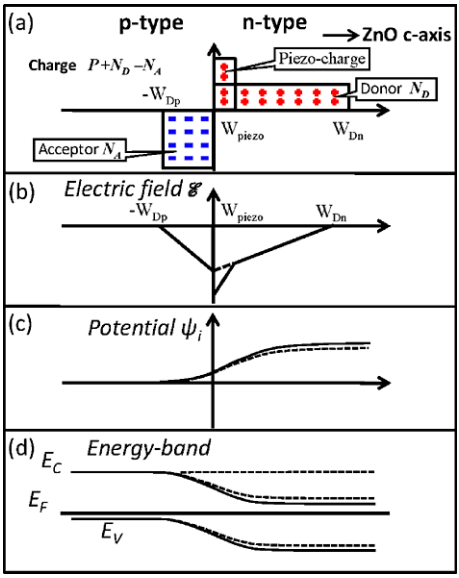

Fig. 3.5 Piezoelectric p–n junction with the presence of piezoelectric charges at applied voltage $V = 0$ (thermal equilibrium). (**a**) Piezoelectric charges, acceptor and donor charges distribution; (**b**) electric field; (**c**) potential distribution and (**d**) energy band diagram with the presence of piezoelectric charges. *Dashed lines* indicate electric field, potential and energy band in the absence of piezoelectric charges, and the *solid lines* are for the cases when a piezopotential is present at the n-type side

material, because the region within which the piezoelectric polarization charge distributes is much smaller than the volume of the bulk crystal, so it is reasonable to assume that the piezoelectric charges are distributed at a surface of zero thickness. But such an assumption is not valid for nanodevices and even microdevices. We assume that the piezoelectric charges distribute at the interface of the p–n junction within a width of W_{piezo} (Fig. 3.5(a)).

We use an abrupt junction model, in which the impurity concentration in a p–n junction changes abruptly from acceptor N_A to donor N_D, as shown in Fig. 3.5(a). The electrons and holes in the junction region form a charge depletion zone, which is assumed to have a box profile. We first calculate the electric field and potential distribution inside the p–n junction. For one-dimensional device, the Poisson equation (3.1) reduces to

$$-\frac{d^2\psi_i}{dx^2} = \frac{dE}{dx} = \frac{\rho(x)}{\varepsilon_s} = \frac{1}{\varepsilon_s}\left[qN_D(x) - qn(x) - qN_A(x) + qp(x) + q\rho_{\text{piezo}}(x)\right] \tag{3.6}$$

where $N_D(x)$ is the donor concentration, $N_A(x)$ is the acceptor concentration, and $\rho_{\text{piezo}}(x)$ is density of polarization charges (in units of electron charge). W_{Dp} and W_{Dn} are defined to be the depletion-layer widths in the p-side and the n-side, respectively. The electric field is then obtained by integrating the above equations, as shown in Fig. 3.5(b):

$$E(x) = -\frac{qN_A(x + W_{Dp})}{\varepsilon_s}, \quad \text{for } -W_{Dp} \le x \le 0, \tag{3.7a}$$

$$E(x) = -\frac{q[N_D(W_{Dn} - x) + \rho_{\text{piezo}}(W_{\text{piezo}} - x)]}{\varepsilon_s}, \quad \text{for } 0 \le x \le W_{\text{piezo}}, \tag{3.7b}$$

$$E(x) = -\frac{qN_D}{\varepsilon_s}(W_{Dn} - x), \quad \text{for } W_{\text{piezo}} \le x \le W_{Dn}. \tag{3.7c}$$

The maximum field E_m that exists at $\mathbf{x} = 0$ is given by

$$|E_m| = \frac{q(N_D W_{Dn} + \rho_{\text{piezo}} W_{\text{piezo}})}{\varepsilon_s}. \tag{3.8}$$

The potential distribution $\psi_i(x)$ is (as shown in Fig. 3.5(c))

$$\psi_i(x) = \frac{qN_A(x + W_{Dp})^2}{2\varepsilon_s}, \quad \text{for } -W_{Dp} \le x \le 0, \tag{3.9a}$$

$$\psi_i(x) = \psi_i(0) + \frac{q}{\varepsilon_s}\left[N_D\left(W_{Dn} - \frac{x}{2}\right)x + \rho_{\text{piezo}}\left(W_{\text{piezo}} - \frac{x}{2}\right)x\right], \quad \text{for } 0 \le x \le W_{\text{piezo}}, \tag{3.9b}$$

$$\psi_i(x) = \psi_i(W_{\text{piezo}}) - \frac{qN_D}{\varepsilon_s}\left(W_{Dn} - \frac{W_{\text{piezo}}}{2}\right)W_{\text{piezo}} + \frac{qN_D}{\varepsilon_s}\left(W_{Dn} - \frac{x}{2}\right)x, \quad \text{for } W_{\text{piezo}} \le x \le W_{Dn}. \tag{3.9c}$$

Thus, the built-in potential ψ_{bi} is given by

$$\psi_{bi} = \frac{q}{2\varepsilon_s}\left(N_A W_{Dp}^2 + \rho_{\text{piezo}} W_{\text{piezo}}^2 + N_D W_{Dn}^2\right). \tag{3.10}$$

Equation (3.10) presents the change in built-in potential as a result of piezoelectric charges due to tensile or compressive straining that defines the sign of the local piezoelectric charges. It is apparent that the piezopotential can change the semiconductor energy band relative to the Fermi level.

Next, we analyze the current–voltage characteristics of a piezoelectric p–n junction by using Shockley theory, which models an ideal junction based on four assumptions: (1) a piezoelectric p–n junction has an abrupt depletion layer; (2) piezoelectric semiconductors are nondegenerate so that the Boltzmann approximation applies; (3) the injected minority carrier concentration is smaller than the majority-carrier concentration so the low-injection assumption is valid; and (4) no generation-recombination current exists inside the depletion layer, and the electron and hole currents are constant throughout the p–n junction. If the width of the piezo-charges is much less than the width of the depletion zone, e.g., $W_{\text{piezo}} \ll W_{Dn}$, the effect of piezoelectric charges on ZnO energy band is considered as a perturbation. The total current density can be obtained by solving (3.2):

$$J = J_p + J_n = J_0\left[\exp\left(\frac{qV}{kT}\right) - 1\right] \tag{3.11}$$

where the saturation current

$$J_0 = \frac{qD_p p_{no}}{L_p} + \frac{qD_n n_{po}}{L_n},$$

p_{no} is the thermal equilibrium hole concentration in n-type semiconductor and n_{po} is the thermal equilibrium electron concentration in p-type semiconductor, and L_p and L_n are diffusion lengths of electrons and holes, respectively. The intrinsic carrier density n_i is given by

$$n_i = N_C \exp\left(-\frac{E_C - E_i}{kT}\right) \tag{3.12}$$

where N_C is the effective density of states in the conduction band, E_i is the intrinsic Fermi level, and E_C is the bottom edge of the conduction band.

For the simple case in which the n-type side has an abrupt junction with donor concentration N_D, and locally $p_{n0} \gg n_{p0}$, we have $J_0 \approx \frac{qD_p p_{no}}{L_p}$, where $p_{no} = n_i \exp(\frac{E_i - E_F}{kT})$, the total current density is given by

$$J = J_0\left[\exp\left(\frac{qV}{kT}\right) - 1\right] = \frac{qD_p n_i}{L_p}\exp\left(\frac{E_i - E_F}{kT}\right)\left[\exp\left(\frac{qV}{kT}\right) - 1\right]. \tag{3.13}$$

If J_{C0} and E_{F0} are defined to be the saturation current density and the Fermi level with the absence of piezopotential,

$$J_{C0} = \frac{qD_p n_i}{L_p}\exp\left(\frac{E_i - E_{F0}}{kT}\right). \tag{3.14}$$

According to (3.9a)–(3.9c), and (3.10), the Fermi lever E_F with the presence of piezopotential is given by

$$E_F = E_{F0} - \frac{q^2 \rho_{\text{piezo}} W_{\text{piezo}}^2}{2\varepsilon_s}. \tag{3.15}$$

Substituting (3.14) and (3.15) into (3.13), we obtain the current–voltage characteristics of the piezoelectric p–n junction [9]:

$$J = J_{C0}\exp\left(\frac{q^2 \rho_{\text{piezo}} W_{\text{piezo}}^2}{2\varepsilon_s kT}\right)\left[\exp\left(\frac{qV}{kT}\right) - 1\right]. \tag{3.16}$$

This means that the current transported across the p–n junction is an exponential function of the local piezo-charges, the sign of which depends on the strain. Therefore, the current to be transported can be effectively tuned or controlled not only by the magnitude of the strain, but also by the sign of the strain (tensile vs. compressive). This is the mechanism of the p–n junction-based piezotronic transistor.

3.5.2 Metal–Semiconductor Contact

The M–S contact is an important component in electronic devices. Similar to our analysis to the piezoelectric p–n junction, the M–S contact can be simplified in the

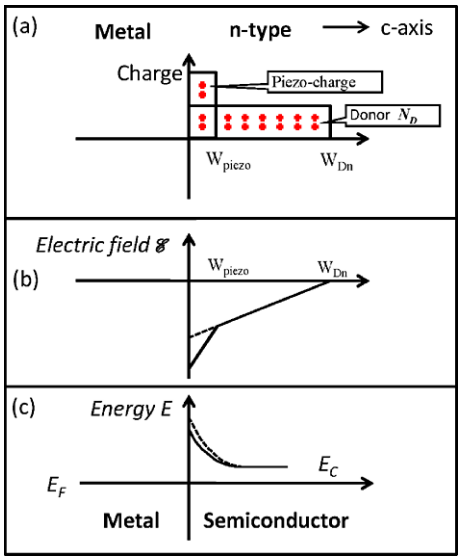

Fig. 3.6 Ideal metal–semiconductor Schottky contacts with the presence of piezoelectric charges at applied voltage $V = 0$ (thermal equilibrium). (**a**) Space charges distribution; (**b**) electric field and (**c**) energy band diagram with the presence of piezoelectric charges. *Dashed lines* indicate electric field and energy band in the absence of piezoelectric charges, and the *solid lines* are for the cases when a piezopotential is present in the semiconductor

charge distribution as shown in Fig. 3.6(a) in the presence of a Schottky barrier. The semiconductor side is assumed to be n-type, and the surface states and other anomalies are ignored for simplification. Under straining, the created piezo-charges at the interface not only change the height of the Schottky barrier, but also its width. Different from the method of changing the SBH by introducing dopants at the semiconductor side, the piezopotential can be *continuously* tuned by strain for a fabricated device.

There are several theories for the M–S Schottky contact, including thermionic-emission theory, diffusion theory and thermionic-emission-diffusion theory. Although the diffusion model is taken as an example for clearly describe the mechanism of piezotronic effect in this paper, the presented methodology also applies to thermionic-emission and thermionic-emission-diffusion model, etc.

The carrier transport in M–S contact is dominated by the majority carriers. The current density equation (3.2) can be rewritten as

$$J = J_n = q\mu_n n E + q D_n \frac{dn}{dx} \tag{3.17}$$

where

$$E = \frac{d\psi_i}{dx} = \frac{dE_c}{dx}.$$

According to the diffusion theory by Schottky, the solutions under forward bias (metal is positive bias) can be obtained as [15]

$$J_n \approx J_D \exp\left(-\frac{q\phi_{Bn}}{kT}\right)\left[\exp\left(\frac{qV}{kT}\right) - 1\right] \tag{3.18}$$

where

$$J_D = \frac{q^2 D_n N_C}{kT} \sqrt{\frac{2qN_D(\psi_{bi} - V)}{\varepsilon_s}} \exp\left(-\frac{q\phi_{Bn}}{kT}\right)$$

is the saturation current density. We define J_{D0} is the saturation current density in the absence of piezoelectric charges:

$$J_{D0} = \frac{q^2 D_n N_C}{kT} \sqrt{\frac{2qN_D(\psi_{bi0} - V)}{\varepsilon_s}} \exp\left(-\frac{q\phi_{Bn0}}{kT}\right) \tag{3.19}$$

where ψ_{bi0} and ϕ_{Bn0} are built-in potential and Schottky-barrier height in the absence of piezoelectric charges. In our case, the effect of piezoelectric charge can be considered as a perturbation to the conduction-band edge E_C. The change in effective Schottky-barrier height induced by piezoelectric charges can be derived from the potential distribution equations (3.9a)–(3.9c), and (3.10):

$$\phi_{Bn} = \phi_{Bn0} - \frac{q^2 \rho_{\text{piezo}} W_{\text{piezo}}^2}{2\varepsilon_s}. \tag{3.20}$$

Thus, the current density can be rewritten as

$$J_n \approx J_D \exp\left(\frac{q^2 \rho_{\text{piezo}} W_{\text{piezo}}^2}{2\varepsilon_s kT}\right)\left[\exp\left(\frac{qV}{kT}\right) - 1\right]. \tag{3.21}$$

This means that the current transported across the M–S contact is an exponential function of the local piezo-charges, the sign of which depends on the strain. Therefore, the current to be transported can be effectively tuned or controlled by not only the magnitude of the strain, but also by the sign of the strain (tensile vs. compressive). This is the mechanism of the piezotronic transistor for M–S case.

3.5.3 Metal–Wurtzite Semiconductor Contact

We now expand the result received in Sect. 3.4 for a special case of metal–wurtzite semiconductor contact, such as Au–ZnO or Ag–ZnO. For the ZnO nanowire grown along c-axis, the piezocoefficient matrix is written as

$$(\mathbf{e})_{ijk} = \begin{pmatrix} 0 & 0 & 0 & 0 & e_{15} & 0 \\ 0 & 0 & 0 & e_{15} & 0 & 0 \\ e_{31} & e_{31} & e_{33} & 0 & 0 & 0 \end{pmatrix}.$$

If the created strain is strain s_{33} along the c-axis, the piezoelectric polarization can be obtained from (3.4) and (3.5):

$$P_z = e_{33} s_{33} = q\rho_{\text{piezo}} W_{\text{piezo}}. \tag{3.22}$$

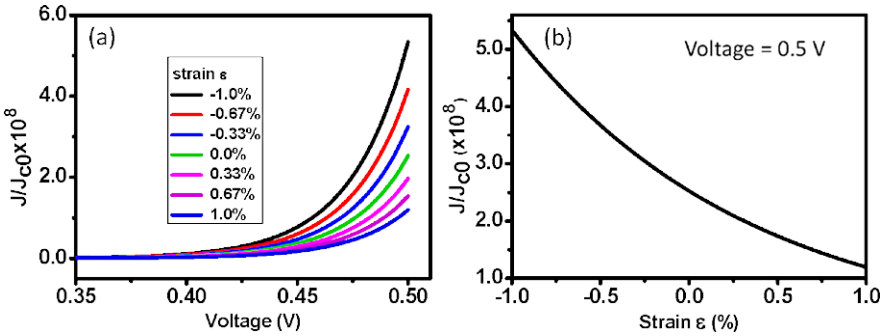

Fig. 3.7 The current–voltage characteristics of an ideal metal–semiconductor Schottky contact in the presence of piezoelectric charges. (**a**) Current–voltage curves at various strain from −1 % to 1 %; (**b**) relative current density as a function of strain at a fixed forward bias voltage of 0.5 V

The current density is

$$J = J_{D0} \exp\left(\frac{q e_{33} s_{33} W_{\text{piezo}}}{2\varepsilon_s kT}\right)\left[\exp\left(\frac{qV}{kT}\right) - 1\right]. \tag{3.23}$$

It is clear that the current transported across the M–S interface is directly related to the exponential of the local strain, which means that the current can be tuned on or off by controlling strain.

For numerical calculation, the material constants are piezoelectric constants $e_{33} = 1.22\ \text{C/m}^2$ and relative dielectric constant is $\varepsilon_s = 8.91$. The width of the piezocharges is $W_{\text{piezo}} = 0.25$ nm. The temperature is $T = 300$ K. Figure 3.7(a) shows the calculated J/J_{D0} as a function of the externally applied voltage V across the M–S interface as a function of the strain, clearly demonstrating its tuning effect on the transported current. When the external voltage is fixed at $V = 0.5$ V at forward bias, J/J_{D0} decreases when the strain changes from −1 % to 1 % (Fig. 3.7(b)). The theoretical result agrees qualitatively with our previous experiments. For reverse bias case, the dominant voltage dependence is mainly due to the change of Schottky barrier in our model.

3.6 Numerical Simulation of Piezotronic Devices

3.6.1 Piezoelectric p–n Junctions

The analytical solutions for one-dimensional simplified cases provide qualitative guidance for understanding the mechanism of how the piezopotential tunes/controls the carrier transport behavior. For a general case, the basic equations of piezotronic device can be solved numerically. For example, with considering the recombination of carriers in the depletion layer, we demonstrate the basic numerical method for simulating piezoelectric p–n junction.

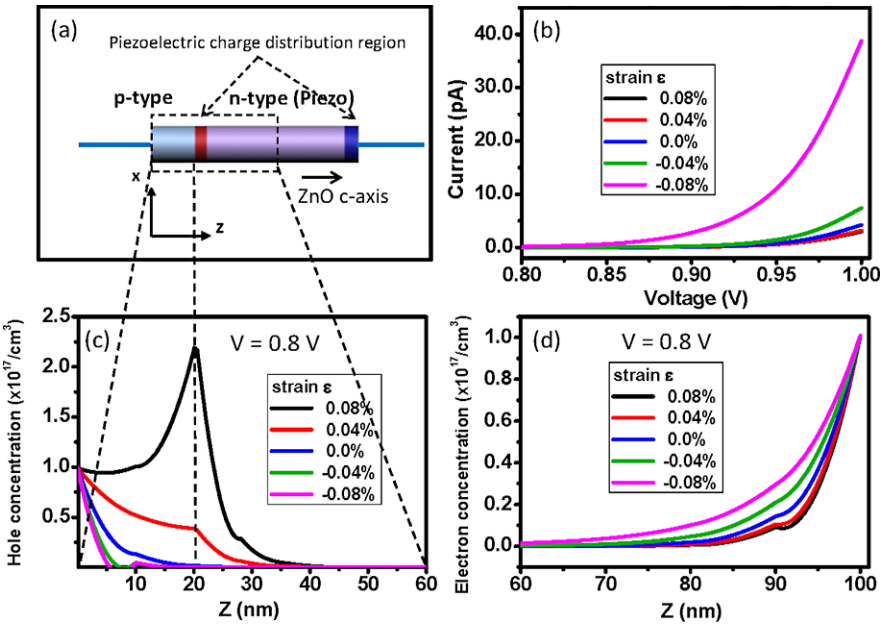

Fig. 3.8 (**a**) Schematic of a piezotronic ZnO nanowire p–n junction; (**b**) calculated current–voltage curves; (**c**) distribution of holes and (**d**) distribution of electrons at a fixed forward bias voltage of 0.8 V across the p–n junction under various applied strain (−0.09 % to 0.09 %) [9]

We first study the DC characteristics of the p–n junction with uniform strain. The piezoelectric charge distribution is obtained by numerically solving (3.4) and (3.5). Then the electrostatic equation, the convection and diffusion equations, and continuity equations are solved using the COMSOL software package. The electrical contacts at the ends of the p–n junction are assumed to be ideal Ohmic contacts, the Dirichlet boundary conditions are adopted for the carrier concentration and electrical potential at the device boundaries [19]. Figure 3.8(a) shows a sketch of a piezotronic nanowire p–n junction to be used for the calculation.

In order to have a reasonable comparison to a p–n junction diode, the dopant concentration function n can be approximately descried using Gaussian functions:

$$N = N_{Dn} + N_{Dn\max} e^{-(\frac{z-l}{ch})^2} - N_{Ap\max} e^{-(\frac{z}{ch})^2} \tag{3.24}$$

where N_{Dn} is the n-type background doping concentration due to the presence of intrinsic defects, $N_{Dn\max}$ is the maximum donor doping concentration and $N_{Ap\max}$ is the maximum acceptor doping concentration, l is the length of ZnO nanowire, ch controls the spreads width of the doping concentration. N is assigned to have a negative value in p-type region and a positive value in n-type region.

There is no external optical excitation in our model so that the electron and hole generation rates $G_n = G_p = 0$. For electron-hole recombination, there are two important recombination mechanisms, including band-to-band recombination and

trap-assisted recombination (named Shockley–Read–Hall recombination). Band-to-band recombination describes the energy transition from conduction band to the valence band by a radiation process (photon emission) or by transfer to another free electron or hole (Auger process). The Shockley–Read–Hall recombination is a general recombination process by traps in the forbidden band gap of the semiconductor. Taking it as an example in our model, the Shockley–Read–Hall recombination is given by

$$U_p = U_n = U_{\mathrm{SRH}} = \frac{np - n_i^2}{\tau_p(n + n_i) + \tau_n(p + n_i)} \tag{3.25}$$

where τ_p and τ_n are the carrier lifetimes. Thus, the basic semiconductor equations (3.1) and (3.3) are rewritten as

$$\begin{cases} \varepsilon_s \nabla^2 \psi_i = -q(p - n + N + \rho_{\mathrm{piezo}}), \\ -\nabla \cdot \mathbf{J}_n = -qU_{\mathrm{SRH}}, \\ -\nabla \cdot \mathbf{J}_p = -qU_{\mathrm{SRH}}. \end{cases} \tag{3.26}$$

For boundary conditions in contact with a metal electrode, the electrostatic potential is a constant. We assume infinite recombination velocity and no charge at the contact. Under an applied voltage, the electrostatic potential at the electrode is the potential corresponding to the quasi Fermi level plus the applied voltage V. The electrostatic potential and carrier concentrations at the electrode are given by [14–17, 20]:

$$\psi = V + \frac{q}{kT} \ln\left(\frac{\frac{N}{2} + \sqrt{(\frac{N}{2})^2 + n_i^2}}{n_i} \right), \tag{3.27a}$$

$$n = \frac{N}{2} + \sqrt{\left(\frac{N}{2}\right)^2 + n_i^2}, \tag{3.27b}$$

$$p = -\frac{N}{2} + \sqrt{\left(\frac{N}{2}\right)^2 + n_i^2}. \tag{3.27c}$$

Thus, we can calculate the above equations to obtain the boundary conditions of the electrostatic potential and carrier concentrator at the electrode.

In our simulation, we choose ZnO as the piezoelectric semiconductor material. The length and radius of the nanowire device are 100 nm and 10 nm, respectively. The p-type is assumed non-piezoelectric here so that it is not restricted to the wurtzite family. For simplicity, we neglect the difference in band gap between the p-type semiconductor and ZnO. The length of the p-type is 20 nm and the length of n-type ZnO is 80 nm. The relative dielectric constants are $\kappa_{\perp}^r = 7.77$ and $\kappa_{//}^r = 8.91$. The intrinsic carrier density is $n_i = 1.0 \times 10^6$ cm^{-3}. The electron and hole mobilities are $\mu_n = 200$ cm^2/V s and $\mu_p = 180$ cm^2/V s. The carrier lifetimes are $\tau_p = 0.1$ μs and $\tau_n = 0.1$ μs. The n-type background doping concentration is $N_{Dn} = 1 \times 10^{15}$ cm^{-3}. The maximum donor doping concentration

is $N_{Dn\max} = 1 \times 10^{17}$ cm^{-3} and the maximum acceptor doping concentration is $N_{Ap\max} = 1 \times 10^{17}$ cm^{-3}. The control constant $ch = 4.66$ nm. The temperature is $T = 300$ K. The piezoelectric charges are assumed to distribute uniformly at the two ends of the n-type segment within a region of 0.25 nm, as represented schematically by red and blue colored zones in Fig. 3.8(a). For easy of labeling, a z-axis is defined in Fig. 3.8(a), with $z = 0$ representing the end of the p-type. The p–n junction is located at $z = 20$ nm along the axis. The n-type ends at $z = 100$ nm.

The current–voltage curves at various strains are shown in Fig. 3.8(b). As for the negative strain (compressive strain) case in our model, the positive piezoelectric charges are at the p–n interface side, which attract the electrons to accumulate toward the p–n junction, resulting in a reduced built-in potential adjacent to the p–n junction. Thus, the corresponding saturation current density increases at a fixed bias voltage. Alternatively, for the positive strain (tensile strain) case, negative piezoelectric charges are created adjacent to the p–n interface, which attract the holes to the local region, resulting in an increase in the built-in potential and dropping in saturation current. Figure 3.8(c) show the distribution of hole concentrations at various strains from -0.08 % to 0.08 % at an applied voltage of $V = 0.8$ V, clearly displaying the effect of piezoelectric charges on the hole distribution. Under tensile strain, the hole concentration shows a peak right at the p–n junction interface where the negative piezoelectric charges accumulate. When a compressive strain is applied, the local positive piezoelectric charges push the holes away from the p–n junction, resulting in a disappearance of the peak. Correspondingly, Fig. 3.8(d) shows the electron distribution in the device at various strains from -0.08 % to 0.08 % at $V = 0.8$ V, showing a slight tendency of increasing. Since the right-hand electrode is an Ohmic contact ($z = 100$ nm), the carriers fully screen the piezoelectric charges at the contact. The electron concentration is rather low adjacent to the p–n junction. The piezoelectric charges at the p–n interface dominate the transport process. Therefore, the piezotronic effect is the result of tuning/controlling the carrier distribution by the device by the generated piezoelectric charges at the two ends.

Using our model, we also studied the DC characteristics and the carrier concentration distribution at various doping concentrations. The strain is fixed at -0.08 % and the n-type background doping concentration N_{Dn} is set to be 1×10^{15} cm^{-3}. By choosing $N_{Dn\max} = N_{Ap\max}$ and increasing $N_{Dn\max}$ from 1×10^{16} to 9×10^{16} cm^{-3}, the corresponding calculated current–voltage curves are plotted in Fig. 3.9(a). When the width of the depletion zone is fixed, the built-in potential increases with $N_{D\max}$. Therefore, the threshold voltage increases, which pushes the "take off" point of the I–V curve moving it to higher voltage. Then, by assuming $N_{Dn\max} = N_{Ap\max} = 1 \times 10^{17}$ cm^{-3} and increasing N_{Dn} from 5×10^{13} to 1×10^{15} cm^{-3}, the I–V curve shows little change, as shown in Fig. 3.9(b). The numerical results indicate that the DC characteristics depend on the distributions of donors and acceptor doping concentration in our model. Furthermore, the distributions of holes and electrons at an applied voltage of 0.8 V are shown in Figs. 3.9(c) and 3.9(d), respectively.

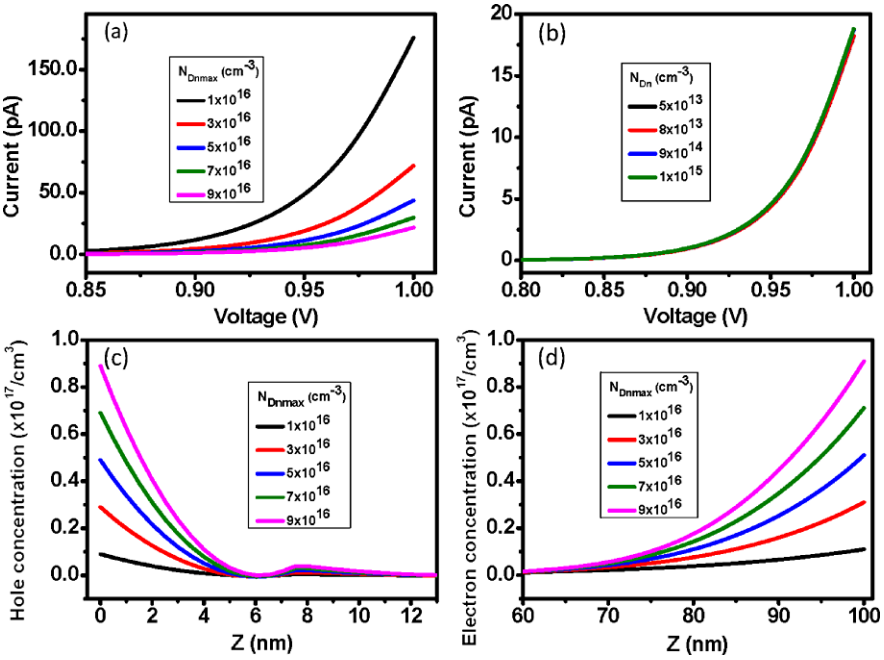

Fig. 3.9 (**a**) Calculated piezoelectric p–n junction current–voltage curves at various maximum donor doping concentration and maximum donor acceptor doping concentration; (**b**) calculated current–voltage curves at various n-type background doping concentration; (**c**) and (**d**) distributions of hole and electron concentrations along the length of the device at an applied forward voltage of 0.8 V at various maximum donor doping concentrations and maximum donor acceptor doping concentrations, respectively [9]

3.6.2 Piezoelectric Transistor

The M–S–M ZnO nanowire devices are the typical piezoelectric transistor in our experimental studies. Using FEM, we solved the basic equations of the M–S–M ZnO nanowire device with the applied strain along the nanowire length direction (*c*-axis). There are many types of M–S–M ZnO nanowire device, including different types of M–S contact and doping profile, etc. M–S contact can be fabricated as Ohmic contact or Schottky contact. The doping profile can be approximated as a box profile or a Gaussian distribution profile, etc. Our calculations are done based on a device model that has the following device property assumptions: the surface states in ZnO are ignored; the electrostatic potential are constants at the end electrodes; the nanowire is n-type without p-type doping; the doping concentration N is approximately descried using a Gaussian function; and, at equilibrium, the electron concentration at the metal contact is unaffected by the transported current; infinite recombination velocity and no charge at the contact. Although the M–S–M ZnO nanowire devices model is taken as a simplified model for clearly describing the mechanism of piezopotential tuning to carrier transport process, the basic principle

also applies to more complex cases, such as different surface states, arbitrary doping profiles and different piezoelectric semiconductor materials, etc.

Using the COMSOL software package, the piezoelectric equations (see (3.4)) are solved first. Then, the electrostatic equation, the convection and the diffusion equations are solved with the piezoelectric charge distribution provided. The doping concentration function N is approximately descried using a Gaussian function:

$$N = N_{Dn} + N_{Dn\max} e^{-(\frac{z-l}{ch})^2}. \tag{3.28}$$

The boundary conditions of the electrostatic potential at the electrode can be given by

$$\psi = V - \chi_{\mathrm{ZnO}} - \frac{E_g}{2} + \frac{q}{kT} \ln\left(\frac{\frac{N}{2} + \sqrt{(\frac{N}{2})^2 + n_i^2}}{n_i} \right) \tag{3.29}$$

where the electron affinity χ_{ZnO} of ZnO is 4.5 eV, and its band gap E_g is 3.4 eV. We assume the carrier concentration at the electrode to be the same as the value at thermal equilibrium. The boundary conditions of the carrier concentration at the electrode can be given by (3.27b).

We calculated the DC transport property of a M–S–M ZnO nanowire device with the presence of piezoelectric charges with the applied strain from -0.39 % to 0.39 %. Figure 3.10(a) shows the sketch of a piezotronic ZnO nanowire device. We choose $l = 50$ nm, which is half the length of the nanowire. The current–voltage curves are shown in Fig. 3.10(b). At negative strain (compressive strain), the positive and negative piezoelectric charges are at the left-hand and right-hand M–S contacts, respectively (as shown in Fig. 3.10(a)), which lower and raise the local Schottky-barrier heights at the corresponding contacts. When an external voltage is applied with the left-hand contact at positive bias, the dominant barrier that dictates the current–voltage curve is the reversely biased contact at the right-hand, at which the local barrier height is raised by piezoelectric charges. Thus, the transported current is lowered in comparison to the case of strain-free device. Alternatively, at positive strain (tensile strain) case and under the same biased voltage, by the same token, the I–V curve is largely determined by the M–S contact at the right-hand, which has a lowered barrier height, resulting in an increase in transported current in comparison to the strain-free case. The device displays 'ON' state at 0.39 % strain, and is 'OFF' at -0.39 % strain. Therefore, the piezopotential acts as a 'gate' voltage to tune/control the current of piezoelectric transistor at the M–S interface and the device can be switched "ON" and "OFF" by switching the applied strain, which is the piezotronic FET.

Figure 3.10(c) shows the electron concentration along the device at an applied voltage $V = 0.8$ V. When an external voltage is applied, the piezoelectric charges affect the peak height and position of the electron concentration distribution. With an increase in strain without applying bias voltage, not only the magnitude of the peak of the electron concentration increases, but also the position of the peak shifts from 44.2 to 55.8 nm when the strain varies from -0.39 % to 0.39 %, as shown in Fig. 3.10(d).

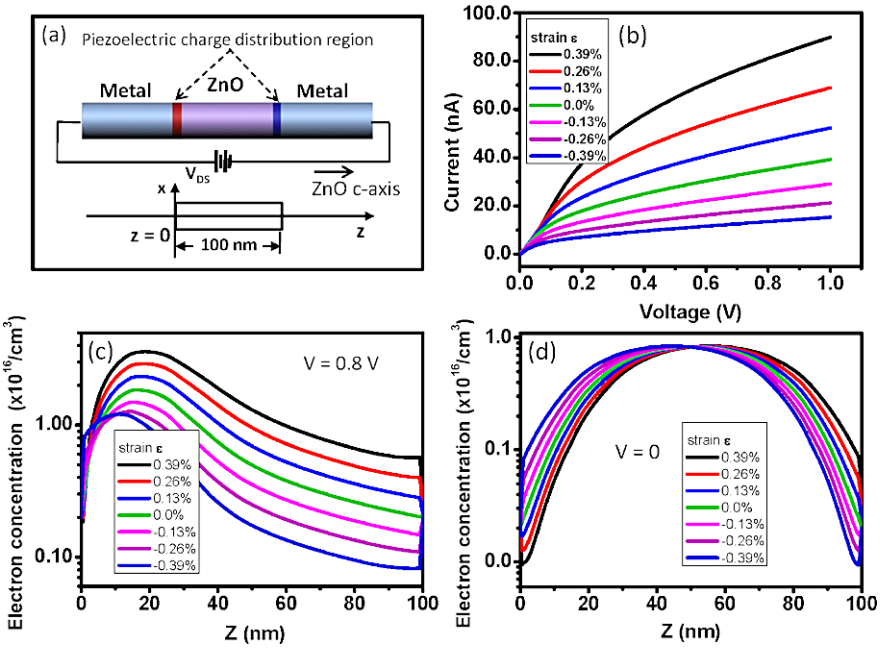

Fig. 3.10 (**a**) Schematic of piezotronic ZnO nanowire transistor; (**b**) calculated current–voltage curves of the device at various applied strain (−0.39 % to 0.39 %); electron distribution in the semiconductor segment (**c**) at a forward voltage of $V = 0.8$ V and (**d**) at $V = 0$ [9]

Furthermore, we study the DC characteristics and the carrier concentration with various doping concentration. In order to investigate how the variance of maximum donor doping concentration and maximum donor acceptor doping concentration affects the DC characteristics, we fix the strain at −0.08 % and the n-type background doping concentration N_{Dn} of 1×10^{15} cm^{-3}. When $N_{Dn\,\max}$ is increased from 1×10^{16} to 9×10^{16} cm^{-3}, the current increases as well (Fig. 3.11(a)). By fixing $N_{Dn\,\max} = N_{Ap\,\max} = 1 \times 10^{17}$ cm^{-3}, the current rises with increasing of N_{Dn} from 1×10^{13} to 1×10^{15} cm^{-3} (Fig. 3.11(b)). The numerical results indicate that the DC characteristics depend on the doping concentration in the piezoelectric transistor. The distribution of electrons at an applied voltage of 0.8 and 0.0 V are shown in Figs. 3.11(c) and (d), respectively.

3.7 Summary

We have presented the theoretical frame of piezotronics by studying the charge transport across the metal–semiconductor contact and p–n junction with the introduction of piezopotential [9]. The analytical solutions derived under simplified conditions are useful for illustrating the major physical pictures of the piezotronic

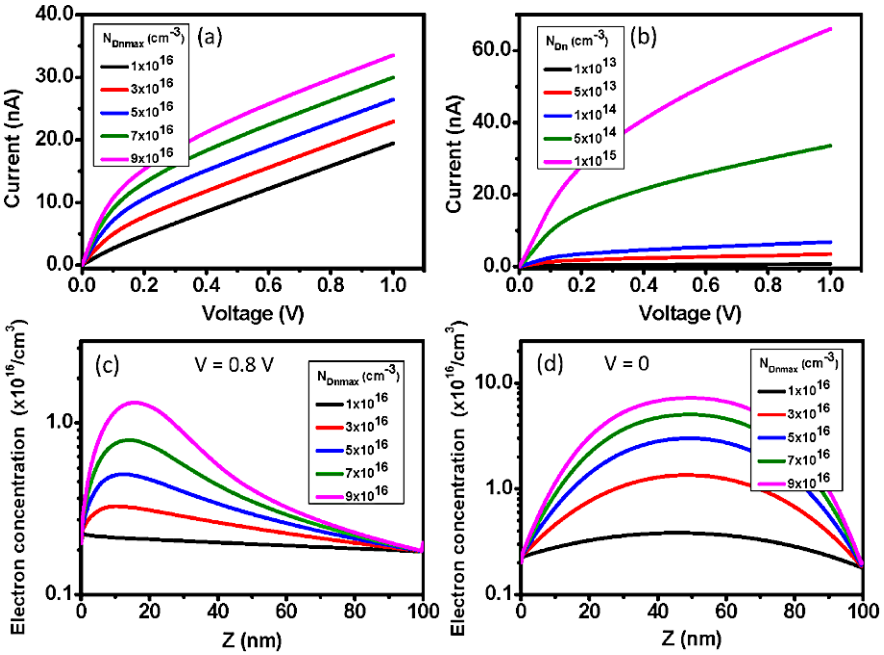

Fig. 3.11 Calculated transport characteristics of a piezotronic ZnO nanowire transistor. (**a**) Piezoelectric M–S–M nanowire transistor current–voltage curves at various maximum donor doping concentrations; (**b**) current–voltage curves at various n-type background doping concentrations; calculated electron distribution in the device at various maximum donor doping concentrations (**c**) at a forward bias of $V = 0.8$ V and (**d**) $V = 0$

devices, and the numerical calculated results are meant for understanding the transport characteristics of the piezotronic transistors in a practical case. The theory presented here not only establishes the solid physical background of piezotronics, but also provides theoretical support for guiding the experimental design of piezotronic devices.

References

1. Z.L. Wang, J.H. Song, Piezoelectric nanogenerators based on zinc oxide nanowire arrays. Science **312**, 242–246 (2006)
2. X.D. Wang, J.H. Song, J. Liu, Z.L. Wang, Direct-current nanogenerator driven by ultrasonic waves. Science **316**, 102–105 (2007)
3. Y. Qin, X.D. Wang, Z.L. Wang, Microfibre–nanowire hybrid structure for energy scavenging. Nature **451**, 809–813 (2008)
4. X.D. Wang, J. Zhou, J.H. Song, J. Liu, N.S. Xu, Z.L. Wang, Piezoelectric field effect transistor and nanoforce sensor based on a single ZnO nanowire. Nano Lett. **6**(12), 2768–2772 (2006)
5. J.H. He, C.H. Hsin, L.J. Chen, Z.L. Wang, Piezoelectric gated diode of a single ZnO nanowire. Adv. Mater. **19**(6), 781–784 (2007)

6. C.S. Lao, Q. Kuang, Z.L. Wang, M.C. Park, Y.L. Deng, Polymer functionalized piezoelectric-FET as humidity/chemical nanosensors. Appl. Phys. Lett. **90**(26), 262107 (2007)
7. Y.F. Hu, Y.L. Chang, P. Fei, R.L. Snyder, Z.L. Wang, Designing the electric transport characteristics of ZnO micro/nanowire devices by coupling piezoelectric and photoexcitation effects. ACS Nano **4**(2), 1234–1240 (2010)
8. Y.F. Hu, Y. Zhang, Y.L. Chang, R.L. Snyder, Z.L. Wang, Optimizing the power output of a ZnO photocell by piezopotential. ACS Nano **4**(7), 4220–4224 (2010)
9. Y. Zhang, Y. Liu, Z.L. Wang, Fundamental theory of piezotronics. Adv. Mater. **23**(27), 3004–3013 (2011)
10. Z.L. Wang, Piezopotential gated nanowire devices: piezotronics and piezo-phototronics. Nano Today **5**, 540–552 (2010)
11. J. Zhou, P. Fei, Y.D. Gu, W.J. Mai, Y.F. Gao, R.S. Yang, G. Bao, Z.L. Wang, Piezoelectric-potential-controlled polarity-reversible Schottky diodes and switches of ZnO wires. Nano Lett. **8**(11), 3973–3977 (2008)
12. Q. Yang, W.H. Wang, S. Xu, Z.L. Wang, Enhancing light emission of ZnO microwire-based diodes by piezo-phototronic effect. Nano Lett. **11**(9), 4012–4017 (2011)
13. Z.L. Wang, Progress in piezotronics and piezo-phototronics. Adv. Mater. **24**, 4632–4646 (2012)
14. S.M. Sze, *Physics of Semiconductor Devices*, 2nd edn. (Wiley, New York, 1981)
15. W. Schottky, Halbleitertheorie der Sperrschicht. Naturwissenschaften **26**(52), 843 (1938)
16. H.A. Bethe, MIT Radiation Lab. Report, vol. 43-12 (November, 1942)
17. C.R. Crowell, S.M. Sze, Current transport in metal–semiconductor barriers. Solid-State Electron. **9**(11–12), 1035–1048 (1966)
18. T. Ikeda, *Fundamentals of Piezoelectricity* (Oxford University Press, Oxford, 1996)
19. http://www.comsol.com/showroom/gallery/114/
20. S. Selberherr, *Analysis and Simulation of Semiconductor Devices* (Springer, Berlin, 1984)